Sub-barrier fusion of $^{27}Al+^{70,72,73,74,76}Ge$: Evidence for shape transition and structure effects

E. F. Aguilera and J. J. Vega
Centro Nuclear, Instituto Nacional de Investigaciones Nucleares, Apartado Postale 18-1027, México, Distrito Federal, Mexico

J. J. Kolata, A. Morsad,* R. G. Tighe, and X. J. Kong
Physics Department, University of Notre Dame, Notre Dame, Indiana 46556
(Received 10 October 1989)

Fusion excitation functions were obtained for $^{27}Al+^{70,72,73,74,76}Ge$ at energies from about 6 MeV below to 7 MeV above the Coulomb barrier. One-dimensional barrier penetration model calculations with one free parameter yield parameters in good agreement with the systematics for fusion above the barrier. Large low-energy enhancements are observed whose trend suggests the presence of a structural change between $^{70,72}Ge$ and $^{73,74,76}Ge$. Within the context of simple model calculations, this trend is explained as arising from the odd-A structure of ^{73}Ge on one hand, and from a spherical (or oblate) to prolate shape transition between $^{70,72,73}Ge$ and $^{74,76}Ge$, on the other hand.

I. INTRODUCTION

The heavy-ion collision process has shown unexpected facets that have been uncovered by the considerable amount of work, both experimental and theoretical, accumulated during the last decade concerning sub-barrier fusion.[1-5] The enhanced cross sections observed for many systems (with respect to simple barrier penetration models), give evidence for the presence of additional degrees of freedom besides the relative separation between the two reacting nuclei.[1,3] Furthermore, the differences found in the excitation functions as the number of neutrons or protons changes suggest that the structure of the colliding nuclei plays an important role in this kind of reaction.[6-10]

Among all possible phenomena that might be influencing the fusion process below the barrier, the effects of static deformation of target and/or projectile,[11-18] and the effects of the excitation of collective vibrational states in the reacting nuclei[14,19-25] (which thus serve as doorway states for fusion), have been systematically studied and the importance of their role is well established (see Ref. 3 for a review). Other effects that have been considered are dynamical deformation,[26] quasielastic transfer,[22] and neck formation.[1,27]

Recent studies of sub-barrier fusion in the region of compound-nuclear mass near $A \simeq 100$ show large enhancements in the corresponding cross sections.[8,9,28] In this work we present data for the fusion of ^{27}Al with $^{70,72,73,74,76}Ge$ at energies near to and below the Coulomb barrier. Effects due to both static deformation and coupling to vibrational states are expected to be present in these systems. ^{27}Al is in a transition region between prolate (^{25}Mg) and oblate (^{28}Si) shapes.[29,30] Its measured quadrupole moment[31] and $B(E2)$ values[32-34] are a signature for a large static deformation, and the models used to describe it indicate an oblate shape.[30]

The Ge nuclei, on the other hand, have extremely interesting features that make them exciting subjects to study from both experimental and theoretical viewpoints. They belong to a region of weak deformation and are very shape unstable (soft).[35-39] These softness properties have been suggested as a possible explanation for certain peculiar effects observed in the sub-barrier fusion of $^{58,64}Ni+^{74}Ge$ and $^{74}Ge+^{74}Ge$.[40] On the basis of systematic studies of neutron transfer reactions [(p,t) and (t,p)] and Coulomb excitation,[39] polarized deuteron and proton scattering [$(\vec{d},d),(\vec{d},d'),(\vec{p},p),(\vec{p},p')$],[41] and inelastic α scattering,[42] it is possible to assign a nearly spherical nature to the ground and low excited states of ^{70}Ge and ^{72}Ge and a moderately prolate deformation to those in ^{74}Ge and ^{76}Ge. A shape transition between ^{72}Ge and ^{74}Ge is also supported by direct measurements of electron scattering.[43]

Our purpose for this paper is to investigate the possible effects of this shape transition on the sub-barrier fusion cross sections for our systems. We included a ^{73}Ge target in an effort to have a closer look at the transition region. This is perhaps the first system with target and projectile having odd-A for which an analysis of sub-barrier fusion data is reported.

In Sec. II we describe the experimental procedure followed in this work. Some details of the analysis of data and the experimental results are presented in Sec. III. The barrier parameters are determined and a comparative analysis is made of the enhancements observed for the different systems in Sec. IV. In Sec. V the model calculations performed to account for the possible different nuclear shapes are described, and a discussion of the corresponding results is given in Sec. VI. Finally, a summary and the conclusions of this work are given in Sec. VII.

II. EXPERIMENTAL PROCEDURE

Beams of ^{27}Al from the three-stage tandem Van de Graaff facility at the University of Notre Dame were used to bombard targets of $^{70,72,73,74,76}Ge$ at lab energies in the region from 67 to 85 MeV, in steps of 1 MeV. Beam intensities ranged from 1 to 4 particle nanoamperes (pna).

The characteristics of the targets are listed in Table I. Note that for each of the first three even isotopes there were two targets; except for ^{70}Ge, the thicker target was always used to obtain all the experimental data points, while the thinner one was then used to repeat a few points allowing us to check the experimental procedure, particularly the energy-loss correction that we will describe in Sec. III. For the case of ^{70}Ge, the two lowest-energy points, as well as three other points in that region, were obtained with the thinner (and more pure) target.

A recoil velocity spectrometer (see Fig. 1) was used to measure the yields of evaporation residues (ER) that come out in a narrow cone around the beam direction. An electrostatic deflector separates the transmitted beam from the residues (the beam-rejection factor is about 10^6), which are in turn electronically separated from slit-scattered beamlike particles, and/or from reaction products coming from the target backing, by means of a time-of-flight (TOF) energy telescope. This telescope consists of a microchannel-plate detector that gives the first time signal, and a silicon surface barrier (SSB) detector placed at the end of a 1m arm that provides both a time and an energy signal. The transmission probability of the ER through the recoil velocity spectrometer was determined empirically by elastic scattering of ions of similar atomic and mass numbers. To accomplish this, we measured the Rutherford scattering of ^{103}Rh ions on ^{60}Ni at bombarding energies of 42, 39, and 36 MeV and at a laboratory angle of 9.75°. (These three energies covered the range of interest for the recoiling compound nuclei of the fused systems produced in the $^{37}Cl+^{58,60,62,64}Ni$ reactions that we have also investigated.) In order to determine how strongly the transmission depends on the mass of the analyzed products, we also used a ^{81}Br beam at 45 and 42 MeV. No measurable mass dependence was noted over this range. We define the transmission probability as the ratio of the number of particles detected at the SSB detector to that initially traveling within the solid angle determined by the entrance slit of the TOF arm (58 μsr). The experimental

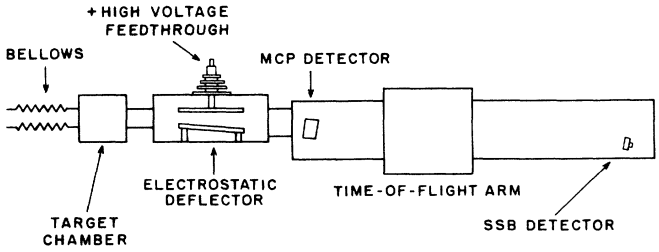

FIG. 1. Schematic side view of the recoil velocity spectrometer.

value of the transmission probability defined in this way was $T=0.780\pm0.045$. As a final check on our transmission determinations, and especially the dependence of the transmission probability on the kinetic energy, charge state distribution, and energy spread of the reaction products, a Monte Carlo model was used to simulate the performance of the spectrometer under different operating conditions. A fairly detailed description of the spectrometer and the transmission measurements was given in Ref. 44, and a more complete report will be published elsewhere. Here it can be said that, as a result of this theoretical analysis, it is known that the transmission is not strongly dependent on any parameters other than the electrostatic rigidity E/q of the ion and the voltage on the deflector. Fortunately, even the latter dependence is weak and the transmission is stable against $\pm5\%$ deviations in the applied voltage for the charge-state distributions and energy spreads that are appropriate to the present experiment.

The simultaneous measurement of Rutherford scattering of the beam with a four-monitor system allowed us to obtain absolute normalization factors for the differential cross sections with high precision ($\sim1\%$). We have shown[45] that, in contrast to the usual method where only one monitor is used (or the less usual one with two monitors), this method gives results that are stable against variations in the equipment-alignment or beam-focusing conditions. Even for the case of reasonably good align-

TABLE I. Characteristics of the targets used in this work. A NO in the third column means a self-supporting target.

Target	Thickness (μg/cm^2)	Carbon backing (μg/cm^2)	Isotropic composition (% of $^{70,72,73,74,76}Ge$)	Notes
^{70}Ge	86 (9)	20	96.75, 1.12, 0.29, 1.36, 0.48	a
	587 (23)	NO	84.62, 5.54, 1.47, 6.36, 2.01	b
^{72}Ge	139 (14)	44	1.04, 96.23, 0.77, 1.63, 0.33	a
	565 (15)	NO		b
^{73}Ge	115 (12)	40	0.86, 2.09, 94.50, 2.24, 0.31	a,c
^{74}Ge	110 (9)	20	1.71, 2.21, 0.90, 94.48, 0.70	a,c
	226 (9)	10		b,c
^{76}Ge	386 (15)	NO	7.69, 6.65, 1.69, 10.08, 73.89	b

[a]Target thickness determined by energy-loss measurements of α particles from an ^{241}Am source.
[b]Target thickness determined by energy-loss measurements of 57.5 MeV ^{16}O ions.
[c]GeO_2.

ment, the precision obtained with our system is typically about 20 (4) times better than that of the 1 (2)-monitor method.[45]

Since particle evaporation is the dominant decay mode for compound nuclei in the present mass and energy range, the complete fusion cross sections were simply taken as the ER cross sections. We measured single-angle excitation functions, at an angle of 3°, which were then normalized to integrated angular distributions obtained at selected energies. As the shape of these angular distributions does not change appreciably within the energy range covered by our experiments, this procedure is well justified.

III. EXPERIMENTAL RESULTS AND DATA ANALYSIS

A typical example of the raw data obtained in these experiments is shown in Fig. 2. In this time-of-flight versus energy plot, the ER island is clearly resolved from the events corresponding to beamlike particles. In Fig. 3, typical angular distributions are presented. Since these distributions are symmetric about $\theta=0°$, the measurement of both positive and negative angles allow for interpolation to the important region of small angles, determining at the same time the 0° position of the time-of-flight arm with high precision. The results of Gaussian fits to the data are shown as continuous curves in Fig. 3. As for the behavior of the widths of the distributions (which were all taken with the corresponding thicker target in Table I), the broadening effects of angular straggling in the target played a more important role than the narrowing effects of an increased neutron excess in the compound nucleus. Integration of the Gaussian distributions over the whole solid angle gave the total fusion cross sections for the selected energies, which were used to scale the single-angle excitation functions.

Energy loss in the target was accounted for in the following way: starting with the bombarding energies in the center-of-mass (c.m.) system, a Wong-type function [see formula (3)] with three free parameters $(R_0, \hbar\omega_0, V_0)$ is fit to the data points (E_n, σ_n). We must mention that for this purpose we do not worry about the physical meaning of the parameters since all that is needed here is an analytical function that represents the data. Calling this function $f_1(E)$, a new energy for the nth point is calculated as the weighted average

$$E_n' = \frac{\int_{E_n}^{E_n^f} E f_1(E)\, dE}{\int_{E_n}^{E_n^f} f_1(E)\, dE} , \tag{1}$$

where E_n^f is the projectile energy after traversing the target. The new data points (E_n', σ_n) produce a second function $f_2(E)$ which, when used instead of $f_1(E)$ in (1), produces in turn a new set of energies. This iterative process is repeated until self-consistent results are obtained.

Impurities in the isotopic composition of the targets were accounted for by solving, for each energy E, the system of linear equations

$$\sigma_m^i(E) = \sum_{j=1}^{5} f_j^i \sigma^j(E), \quad i=1,\ldots,5 , \tag{2}$$

where $\sigma_m^i(E)$ is the measured cross section for the ith target, f^i is the fraction of the jth isotope that is present in the ith target (see Table I), and $\sigma^j(E)$ is the unknown cross section for the jth isotope. Since the energies measured for the different targets differ from each other after

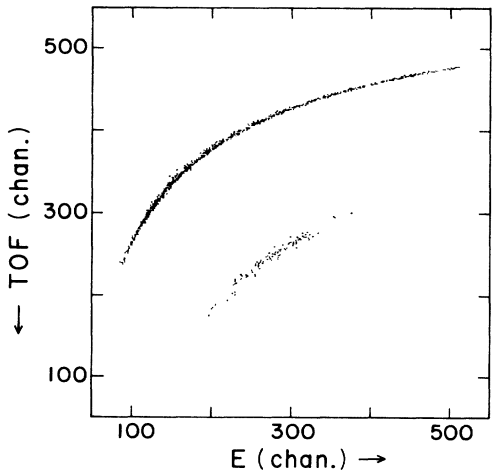

FIG. 2. Scatter plot of the particles detected at 2° in the bombardment of ^{76}Ge with 80 MeV (lab) ^{27}Al. The time of flight (the energy) decreases (increases) linearly with the channel number.

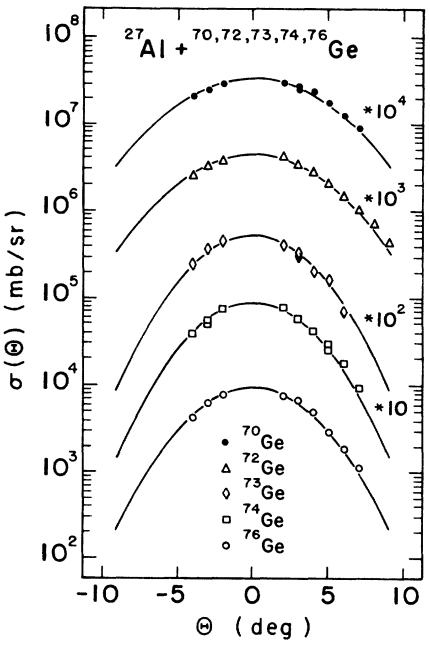

FIG. 3. Angular distributions obtained for ^{27}Al $+^{70,72,73,74,76}$Ge at $E_{\rm c.m.}=56.4$, 56.9, 56.4, 57.8, and 58.0 MeV, respectively. The error bars are smaller than the points in all cases.

energy loss correction, an interpolation procedure was followed in which Wong-type functions were used as described in the previous paragraph.

The resulting fusion cross sections are listed in Table II. The reported errors include the 1% uncertainty in the absolute normalization factors (see Sec. II) and the statistical errors. In addition, a maximum systematic error of about 8% is estimated for our data coming mainly from the transmission efficiency determination ($\sim 6\%$), the scaling of single-angle excitation functions ($\sim 3\%$),

TABLE II. Total fusion cross sections for Al+Ge systems.

System	$E_{c.m.}$ (MeV)	σ_{fus} (mb)	System	$E_{c.m.}$ (MeV)	σ_{fus} (mb)
$^{27}Al+^{70}Ge$	50.2	0.48(13)		56.4	108.4(87)
	50.9	1.16(19)		57.2	135(11)
	51.2	1.44(17)		57.9	157(12)
	51.6	3.12(35)		58.6	166(12)
	51.9	4.78(34)		59.3	210(19)
	52.3	7.47(73)		60.2	242(16)
	52.6	8.31(50)		60.2	250(17)
	53.0	13.4(13)		60.9	271(19)
	53.3	16.83(86)		61.7	319(22)
	53.9	28.0(12)			
	54.5	47.6(20)	$^{27}Al+^{74}Ge$	49.2	0.20(6)
	55.1	62.4(24)		50.0	0.67(13)
	55.8	89.1(33)		50.7	2.18(21)
	56.4	98.6(30)		51.4	6.22(55)
	57.1	134.6(43)		52.1	12.16(75)
	57.8	160.8(54)		52.8	20.8(10)
	58.5	181.1(59)		53.5	35.4(16)
	59.2	224.0(68)		54.2	50.2(20)
	59.2	220.6(82)		54.9	71.9(28)
	59.9	267.8(84)		55.7	89.5(30)
	59.9	255.1(93)		56.4	117.8(39)
				57.1	141.2(47)
$^{27}Al+^{72}Ge$	49.5	0.16(4)		57.8	183(22)
	50.2	0.46(6)		58.6	193.1(65)
	50.9	1.11(12)		59.3	214.4(69)
	51.7	3.29(31)		60.0	235.3(84)
	52.3	7.38(65)		60.8	266.9(88)
	53.0	14.70(52)		61.5	301(12)
	53.7	23.61(85)			
	54.3	39.1(14)	$^{27}Al+^{76}Ge$	48.8	0.14(5)
	54.9	60.8(23)		49.6	0.54(8)
	55.6	79.7(26)		50.3	2.21(25)
	56.2	102.5(32)		51.0	4.21(38)
	56.9	135.8(40)		51.7	9.58(68)
	57.6	160.4(50)		52.4	20.2(12)
	58.3	198.2(66)		53.1	30.9(11)
	59.0	222.6(68)		53.8	48.1(17)
	59.7	223.8(62)		54.5	69.1(25)
	60.4	279.2(84)		55.2	94.3(30)
				55.9	119.3(37)
$^{27}Al+^{73}Ge$	50.0	0.81(18)		56.6	142.4(44)
	50.7	2.54(39)		57.3	184.3(57)
	51.5	5.78(44)		58.0	197.3(62)
	52.2	10.17(58)		58.8	233.1(71)
	52.9	18.9(11)		59.5	261.3(79)
	53.6	26.0(16)		60.2	297.1(90)
	54.4	43.2(23)		61.0	311.7(90)
	55.1	59.5(33)		61.7	364(11)
	55.8	86.2(63)			

and the observation angle of the spectrometer ($\sim 5\%$). Since the corrections for isotopic impurities were very small for most data points, we neglected the corresponding contribution to the systematic error. The data are displayed in Fig. 4 for all systems, together with model calculations that will be discussed in the following sections.

IV. ONE-DIMENSIONAL CALCULATIONS AND COMPARATIVE ANALYSIS

The one-dimensional barrier penetration model (BPM), in one of its more simple versions, predicts fusion cross sections as given by Wong's formula:[46]

$$\sigma_f^0(E,V_0)=\frac{\hbar\omega_0 R_0^2}{2E}\ln\left[1+\exp\left[\frac{2\pi}{\hbar\omega_0}(E-V_0)\right]\right], \quad (3)$$

where E is the energy in the center of mass, R_0 and V_0 are the radius and the height of the barrier, respectively, and $\hbar\omega_0$ is determined by the curvature at the top of the barrier and by the reduced mass μ according to

$$\hbar\omega_0=\left[-\frac{\hbar^2}{\mu}\frac{d^2V(r)}{dr^2}\right]^{1/2}_{r=R_0}. \quad (4)$$

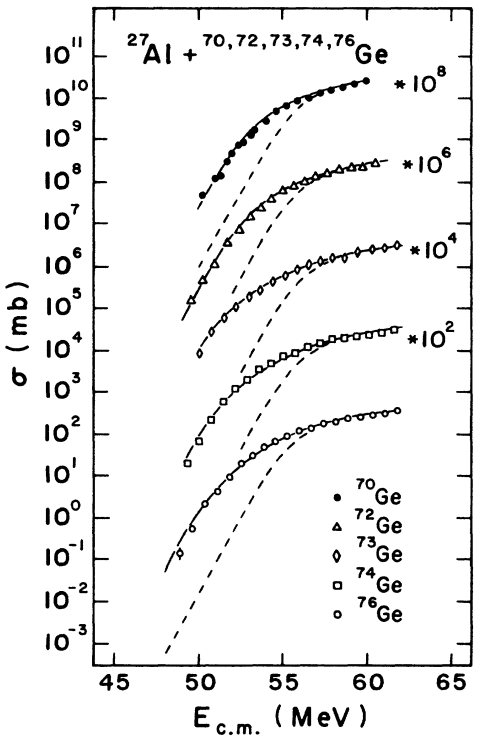

FIG. 4. Experimental fusion cross sections for ^{27}Al $+^{70,72,73,74,76}$Ge. The dashed curves correspond to one-dimensional barrier penetration calculations, while the continuous curves are the results of the "best-model" calculations, as discussed in the text.

Using the Coulomb potential for two point charges plus a nuclear potential of Woods-Saxon shape, a one-parameter fit was made to the data in the region where $\sigma > 100$ mb. According to Vaz *et al.*,[1] this procedure should produce barrier parameters that are nearly independent of the potential assumed. The radius and diffuseness of the Woods-Saxon well were fixed at $R = R_p + R_t + 0.29$ fm and $a = 0.63$ fm, where the projectile and target radii are calculated according to

$$R_{p,t}=1.233A_{p,t}^{1/3}-0.978A_{p,t}^{-1/3}\ \text{fm}, \quad (5)$$

while the depth was varied until the resulting barrier parameters, when inserted into (3), gave the best fit.

These parameters, along with the corresponding results from the systematics reported in Ref. 1, are shown in Table III. We see that the extracted barriers agree with those calculated from Ref. 1 within better than 1%. Considering that the systematic error estimated for our data gives about $\pm 0.6\%$ uncertainty in the barrier heights, we see that both values are within or very near the error bars for all systems.

The corresponding BPM curves are shown as dashed lines in Fig. 4. We immediately see that there is a large enhancement of the sub-barrier cross sections for all systems. In addition, a careful observation indicates a qualitative change in the behavior of the excitation functions between ^{70,72}Ge and ^{73,74,76}Ge. They seem to fall less steeply with decreasing energy for the heavier isotopes, thus giving rise to larger enhancements.

This behavior becomes more evident in the plot of Fig. 5, where the enhancement factors are displayed for each system. Trivial effects of barrier-height shifts between different systems are eliminated here by subtracting from the c.m. energy the respective barrier heights for each system. Three features can be observed in this figure. (1) The flat region with unit ratio for above-barrier energies reminds us that the one-dimensional BPM provides a good description of data in this region. (2) The large deviations from unity for low energies indicate the breakdown of the one-dimensional assumption. (3) The abrupt change in the curves for the three heaviest systems, which grow steeply with decreasing energy leaving a gap between them and those corresponding to the lightest systems, strongly suggests a structural change between ^{70,72}Ge and ^{73,74,76}Ge. On the basis of simplified coupled-channel and equivalent-spheres calculations, we will be able to account for these features in the following sections.

TABLE III. Barrier parameters extracted from our data and from the systematics of Ref. 1.

	This work			Systematics	
System	R_0 (fm)	V_0 (MeV)	$\hbar\omega_0$ (MeV)	R_0 (fm)	V_0 (MeV)
^{27}Al+^{70}Ge	10.2	55.1	3.8	10.0	55.3
^{27}Al+^{72}Ge	10.2	55.1	3.8	10.1	55.0
^{27}Al+^{73}Ge	10.1	55.3	3.8	10.1	54.9
^{27}Al+^{74}Ge	10.1	55.2	3.8	10.1	54.7
^{27}Al+^{76}Ge	10.2	54.6	3.7	10.2	54.5

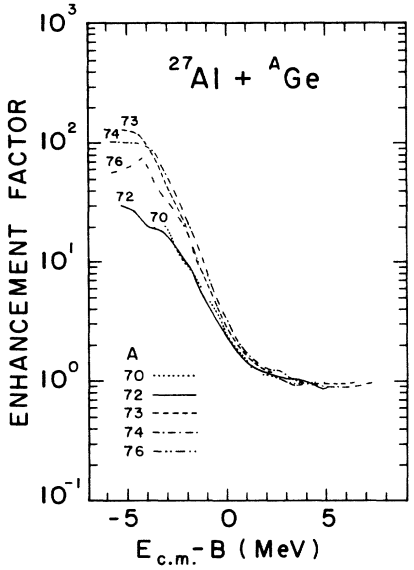

FIG. 5. Enhancement factors for $^{27}Al+^{70,72,73,74,76}Ge$ as a function of the energy excess with respect to the barrier.

V. COUPLED-CHANNEL AND EQUIVALENT-SPHERES CALCULATIONS

In order to account for the possibility of exciting collective degrees of freedom (surface vibrations) of the target and/or projectile on their way to fusion, we used the finite range version of the simplified coupled-channel program CCFUS.[47] In the approach followed in this code, the effect of the coupling is to replace the barrier $V(r)$ by a set of barriers $[V(r)+\lambda_m(r)]$, which confronts the incoming flux. The total transmission is given by a weighted average of the transmission functions for each effective barrier

$$T=\sum_m |U_{m0}|^2 T[E,V(r)+\lambda_m(r)] . \tag{6}$$

The weighting factors U_{m0} and the barrier modification $\lambda_m(r)$ can be determined by diagonalizing the coupling interaction, which depends on the deformation parameters β_λ through the coupling strength

$$\begin{aligned} F_{\text{inel}} &= F_N + F_C , \\ F_N &= -\frac{\beta_\lambda R}{\sqrt{4\pi}} \frac{dV}{dr} , \\ F_C &= \frac{\beta_\lambda R}{\sqrt{4\pi}} \left[\frac{3 z_p z_t e^2}{(2\lambda+1) r^2} \left(\frac{R}{r} \right)^{\lambda-1} \right] . \end{aligned} \tag{7}$$

To calculate the nuclear radius R, relation (5) is used. The fusion cross section then has contributions from several terms of the type given in expression (3):

$$\sigma_f(E)=\sum_m |U_{m0}|^2 \sigma_f^0(E,V_0+\lambda_m) . \tag{8}$$

In a recent version of CCFUS,[48] the possibility of accounting for a static deformation of target and/or projectile has been implemented. The basic idea here is that the nuclear radii of deformed nuclei depend on the deformation parameters and on the orientation angles θ_t with respect to the collision axis. Through them, the nuclear and Coulomb potentials depend also on these variables. Using the method of equivalent spheres,[13,46] a calculation of the type described by (3) or (8) can be performed for each pair (θ_p,θ_t) and the final result is obtained by averaging over all possible orientations.

We were thus able to perform calculations under any of three assumptions for the shape of each reactant: (a) It is spherical, in which case a coupling of the ground state to the inelastic vibrational channels was included, (b) it has a static oblate deformation ($\beta<0$), or (c) it has a static prolate deformation ($\beta>0$). In the latter two cases the above-described method was used without explicitly including any excited state of the reactant.

For any calculation, the input parameters are those related to the barrier on one hand and those describing the inelastic channels to be coupled or the static deformation of the ground state on the other hand. The barrier parameters used were always those determined in Sec. IV (Table III). As for the inelastic channels, all known states with a significant $E2$ or $E3$ transition strength to the ground state were taken into account. The respective spectroscopic information is listed in Table IV, which includes a column with the transition strength $B(E\lambda)$ in Weisskopf units (W.u.) in order to give a better idea of the collective nature of the state. The usual relation[56] between β_λ and $B(E\lambda)$ was used. For calculations where a static deformation had to be entered, the values of $|\beta_2|$ listed in Table IV for the corresponding lowest transition was used in each case, a procedure that can be justified within the adiabatic rotational model under the assumption of an axially symmetric nucleus [the sign of β is undetermined because of its square-root relation with $B(E2)$]. Since it is the deformation length $\beta_\lambda R$ that is the relevant quantity, all values of β_λ given in this paper were normalized to correspond to a standard radius given by (5).

Calculations for all nine combinations of the possible model assumptions for the shape of each nucleus were performed. The following shorthand notation is defined in order to label the different models: Two capital letters are used, the first referring to the projectile and the second to the target. Each letter can be either S, O, or P meaning that a spherical, an oblate deformed, or a prolate deformed shape is assumed for the nucleus, respectively. So, for example, a model calculation where Al is assumed oblate deformed, while Ge is assumed spherical (vibrational) is labeled OS.

VI. DISCUSSION

The results of some selected model calculations for each system are compared with the experimental data and with the respective BPM calculations in Figs. 6–10. From Fig. 6 we already see some very interesting features: Our data for $^{27}Al+^{70}Ge$ cannot be matched if a prolate deformation is assumed for Al. The results for a spherical Al, not displayed in the figure, give an even worse fit. The best of them corresponds to the SS assumption and the corresponding curve has the wrong

TABLE IV. Inelastic channels included in the coupled-channel calculations, and respective coupling parameters.

Nucleus	J^π	E_x (MeV)	λ	$B(E\lambda)_{\text{W.U.}}$	β_λ	Reference
^{27}Al	$\frac{1}{2}^+$	0.84	2	8.1	0.37	49
	$\frac{3}{2}^+$	1.01	2	7.4	0.35	49
	$\frac{7}{2}^+$	2.21	2	14	0.49	49
	$\frac{9}{2}^+$	3.00	2	6.9	0.34	49
^{70}Ge	2^+	1.04	2	21	0.23	39,50,51
	3^-	2.56	3	21.3	0.23	39,52
^{72}Ge	2^+	0.83	2	23.5	0.25	39,51
	3^-	2.51	3	23.7	0.24	39,53
^{73}Ge	$\frac{5}{2}^+$	0.013	2	22.9	0.24	54
	$\frac{7}{2}^+$	0.069	2	41	0.32	54
	$\frac{7}{2}^+$	0.499	2	6.3	0.13	54
	$\frac{13}{2}^+$	0.826	2	30	0.27	54
^{74}Ge	2^+	0.60	2	32	0.29	39,50,51
	3^-	2.54	3	10.2	0.16	53,55
^{76}Ge	2^+	0.56	2	29	0.27	39,50,51
	3^-	2.69	3	8.7	0.14	53,55

slope, underpredicting the high-energy points, while overpredicting the low-energy ones. An oblate Al, combined with either a spherical or an oblate Ge, are clearly the best choices for this system. This is in agreement with what has been concluded from independent spectroscopic studies about both ^{70}Ge (Refs. 39, 41, and 42) and ^{27}Al (Ref. 30) [the positive sign that has been assigned to the measured quadrupole moment of the ground state of ^{27}Al (Refs. 31, 32, and 56) is not in contradiction to a negative intrinsic quadrupole moment (oblate shape), as noted in Ref. 30]. We will now show that a consistent scheme can be obtained by making a global analysis for all measured systems.

For each excitation function, the goodness of fit for a given model calculation can be measured by the quantity

$$\chi=\left\{\frac{1}{N}\sum_{i=1}^{N}\left[\left[\frac{\sigma_{\text{exp}}(E_i)-\sigma_{\text{mod}}(E_i)}{\sigma_{\text{mod}}(E_i)}\right]\Big/e_i\right]^2\right\}^{1/2}, \quad (9)$$

where N is the number of points, E_i are the experimental energies, σ_{exp} and σ_{mod} are the experimental and the model cross sections, respectively, and e_i is the experimental error in σ_{exp} divided by σ_{mod}. In this definition, more importance is given to the relative than to the absolute deviations from the data, which is appropriate since we want to have a good description of the data in the far sub-barrier region.

The values of χ obtained for each system under all different model assumptions are presented in Table V. The sensitivity of this parameter to the goodness of fit can be easily visualized. For example, we see that the two curves OS and OP in Fig. 6 make a difference of about 30% in the respective values of χ. We can now make the following argument: From the first two lines in Table V we can rule out the assumption that ^{27}Al is spherical or prolate since no acceptable fit is obtained under this assumption for the ^{27}Al+^{70,72}Ge systems, a conclusion that was already drawn from Fig. 6 for the first system. As for the ^{70,72}Ge isotopes, we can rule out the assumption of their being prolate, but so far they could be either spherical or oblate since the corresponding fits are nearly equivalent, as seen from the respective χ values and from Figs. 6 and 7.

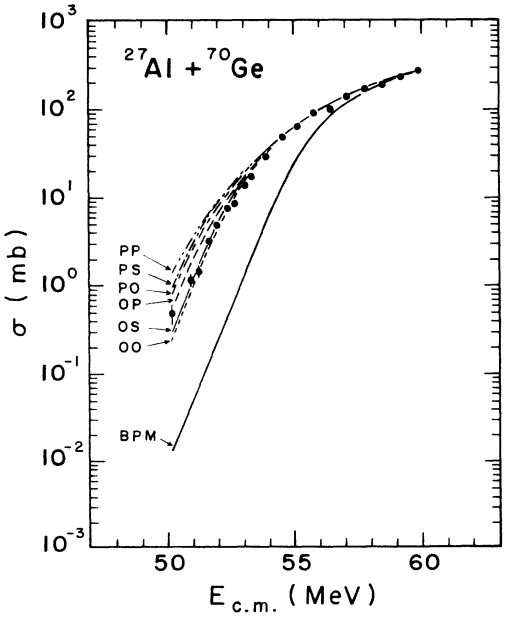

FIG. 6. Comparison of model calculations (curves) with experimental data (dots) for the ^{27}Al+^{70}Ge system. O, P, S in the first (second) place means Al (Ge) oblate, prolate, spherical, respectively. BPM refers to the one-dimensional barrier penetration model calculation.

TABLE V. Value of χ (see text) for the different model predictions for each system. O, P, and S in the first (second) place means Al (Ge) oblate, prolate, and spherical, respectively.

System	Model								
	OO	OP	OS	PO	PP	PS	SO	SP	SS
$^{27}Al+^{70}Ge$	2.19	3.12	2.24	5.10	6.97	6.02	6.50	8.50	3.36
$^{27}Al+^{72}Ge$	2.36	4.29	2.60	5.97	10.0	7.07	7.48	11.9	3.83
$^{27}Al+^{73}Ge$	4.43	3.08	1.03	2.30	1.48	2.62	1.48	0.79	0.99
$^{27}Al+^{74}Ge$	4.43	2.87	4.84	2.92	4.36	3.39	1.79	4.65	4.46
$^{27}Al+^{76}Ge$	3.18	2.40	3.71	2.56	5.39	7.07	2.34	5.98	3.83

We may now go to the third line in Table V and, looking only to the OO, OP, and OS columns, conclude that ^{73}Ge ought to be spherical in order to have consistency with the previous conclusion. The superiority of the OS over the OO and OP models for $^{27}Al+^{73}Ge$ is clearly displayed in Fig. 8. We note here that the relative positions of the three curves has changed with respect to the situation for $^{27}Al+^{70,72}Ge$, Figs. 6 and 7. This illustrates the fact that ^{73}Ge, being an odd nucleus, possesses more low-energy ground-state transitions than the neighboring even nuclei (see Table IV). The additional channels coupled into the calculation increase the enhancement at low energies thus shifting the OS curve higher in Fig. 8. This in turn explains the origin of the structural change between ^{72}Ge and ^{73}Ge suggested by Fig. 5 and discussed in Sec. IV. It is the usual change in structure between an even and an odd nucleus!

From the last two lines in Table V, staying again in the columns corresponding to oblate Al, we see that the data now favor the interpretation that both ^{74}Ge and ^{76}Ge are prolate deformed. Again, this is in agreement with the results of independent spectroscopic studies,[39,41,42] as mentioned in Sec. I. The new situation is displayed in Figs. 9 and 10. We see that, as expected, the relative positions of the OO, OP, and OS curves are qualitatively similar to the corresponding positions for $^{27}Al+^{70,72}Ge$ in Figs. 6 and 7. The quantitative differences can be ascribed to the increased deformation of the heavier isotopes on one hand, which seems to affect the OP calculation more than the OO calculation, and to the decreased strengths of the $E3$ transitions in $^{74,76}Ge$ on the other hand (see Table IV), which lowers the OS curve. The data, however, show now a larger enhancement at the lowest energies, making the OP model the only one able to describe them. Therefore, in this case the structural change suggested by Fig. 5 can actually be ascribed, within the framework of our model calculations, to a shape transition to prolate deformation for $^{74,76}Ge$.

We thus arrive at a scheme where all data can be described within the framework of our simple model calculations if a vibrational character is assumed for $^{70,72,73}Ge$ while a prolate deformation is assigned to $^{74,76}Ge$, using always an oblate deformed ^{27}Al. For $^{70,72}Ge$, an oblate deformation can describe the data equally well. The corresponding model calculations are illustrated by the continuous curves in Fig. 4, where the OS model was used for $^{70,72}Ge$. Only one free parameter, the depth of the nuclear part of the potential, was fit in the BPM calculations and then carried unchanged to the more complete model calculations. The excellent agreement with the data can be fully appreciated in Fig. 4.

The importance of doing a global comparative analysis

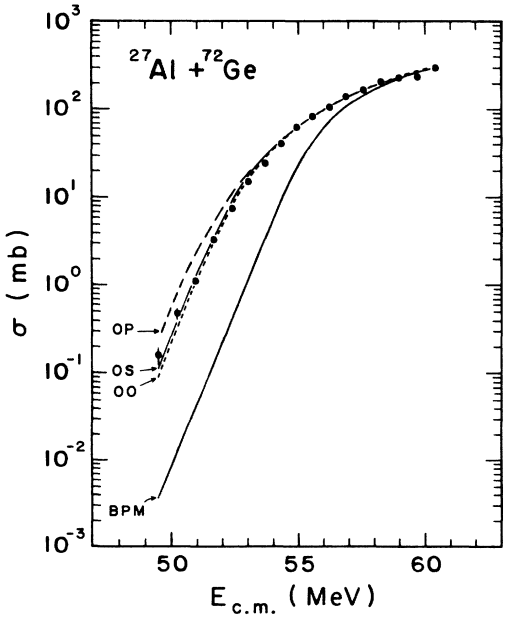

FIG. 7. Same as Fig. 6, but for the $^{27}Al+^{72}Ge$ system.

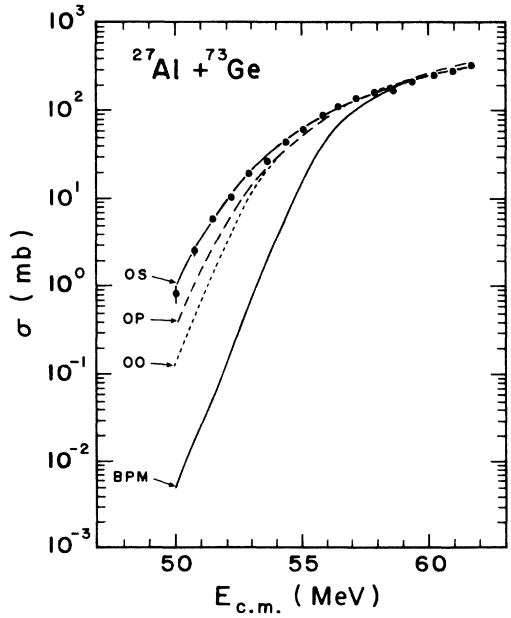

FIG. 8. Same as Fig. 6, but for the $^{27}Al+^{73}Ge$ system.

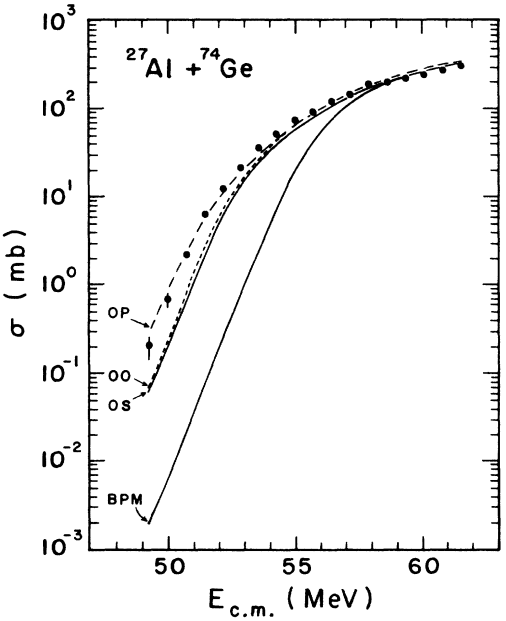

FIG. 9. Same as Fig. 6, but for the ^{27}Al+^{74}Ge system.

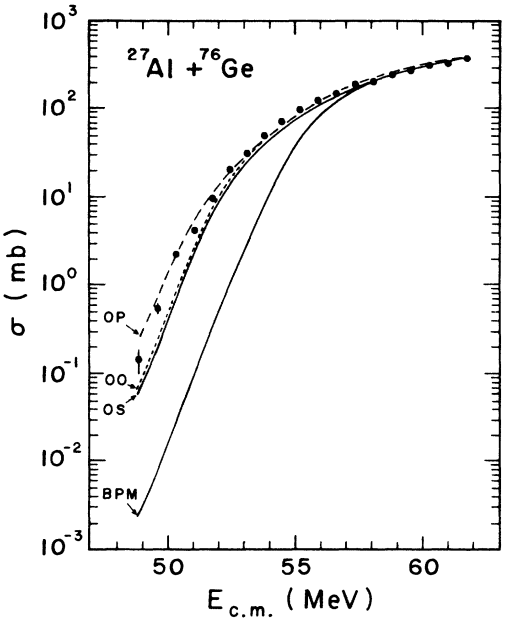

FIG. 10. Same as Fig. 6, but for the ^{27}Al+^{76}Ge system.

as in this work must be emphasized. A naive survey of individual lines in Table V could lead to the model sequence OO, OO, SP, SO, SO for the "best" description of data for ^{27}Al+^{70,72,73,74,76}Ge, respectively. Should we have measured only the three heaviest systems, for example, we could have erroneously concluded that ^{27}Al is spherical, while ^{73}Ge is prolate deformed and both ^{74}Ge and ^{76}Ge are oblate deformed. The use of independent information concerning the oblate nature of Al could fix this problem, of course, but it is only within the framework of the global analysis of many systems that a self-consistent description can be obtained.

VII. SUMMARY AND CONCLUSIONS

The near and sub-barrier fusion cross sections for the ^{27}Al+^{70,72,73,74,76}Ge systems have been measured using a recoil velocity spectrometer. A single-parameter fit of one-dimensional BPM calculations to the cross sections in the region above 100 mb gave barrier parameters for all systems that are in excellent agreement with the existing systematics. Using these parameters, a comparative analysis of the sub-barrier enhancements for all systems was made. This analysis clearly indicates a structural change between ^{70,72}Ge and ^{73,74,76}Ge.

Using systematic calculations in which inelastic vibrational channels are coupled to the ground state of spherical nuclei, while the equivalent-spheres method is used for deformed nuclei, a consistent scheme was found that very neatly described all features of the data. The larger enhancement for ^{27}Al+^{73}Ge with respect to ^{27}Al +^{70,72}Ge was explained as the result of the vibrational ^{73}Ge nucleus having more low-lying collective inelastic channels that can be coupled to the ground state with appreciable strength because of its odd-A nature. For the case of ^{27}Al+^{74,76}Ge, on the other hand, the larger enhancement could be explained as the consequence of a transition from spherical (or possibly oblate) shapes for ^{70,72}Ge to prolate deformed shapes for ^{74,76}Ge. Spectroscopic information from the literature[57,58] was used in these calculations, without any free parameter except for the one mentioned earlier for the BPM calculations.

The scheme arrived at in this work is consistent with that obtained from systematic studies of neutron transfer reactions, Coulomb excitation, deuteron, and proton and α-particle scattering[39,41,42] concerning the Ge isotopes. It is also consistent with information obtained from energy-level spectra, $B(E2)$ values, and nucleon pickup measurements[30] for ^{27}Al. We conclude, therefore, that sub-barrier fusion measurements do actually offer very interesting possibilities for the investigation of nuclear structure.

From the theoretical point of view, it would be interesting to analyze our data within the framework of a more rigorous model than the one used here, which is bound to have limitations in view of its simplifying assumptions. From the experimental point of view, to repeat the measurements on the Ge isotopes using a spherical projectile such as ^{16}O or ^{40}Ca would be of interest since the effects of the differing structure of the Ge isotopes could be isolated in this way.

ACKNOWLEDGMENTS

We would like to thank R. Kryger, G. Murillo, and S. Dixit for their help in data taking. Thanks are also due to Dr. S. Landowne for providing us with the latest version of the CCFUS code. This work was partially supported by Consejo Nacional de Ciencia y Tecnología (CONACyT) (Mexico) under Contract No. 140105 0102-139 and by the U.S. National Science Foundation (NSF) under Contract Nos. 88-03658 and PHY88-03035.

*Present address: Centre de Recherches Nucléaires and Université Louis Pasteur, 67037 Strasbourg CEDEX, France.

[1]L. C. Vaz, J. M. Alexander, and G. R. Satchler, Phys. Rep. **69**, 373 (1981).

[2]*Proceedings of the International Conference on Fusion Reactions Below the Coulomb Barrier, Massachusetts Institute of Tech-*

nology, Cambridge, 1984, Vol. 219 of *Lecture Notes in Physics,* edited by S. G. Steadman (Springer, Berlin, 1985).
[3]M. Beckerman, Phys. Rep. **129**, 145 (1985).
[4]Proceedings of the Symposium on the Many Facets of Heavy-Ion Fusion Reactions, Argonne National Laboratory, 1986, Argonne National Laboratory Report No. ANL-PHY-86-1.
[5]Proceedings of the Symposium on Heavy Ion Interactions Around the Coulomb Barrier, Legnaro, Italy, 1988 (unpublished).
[6]M. Beckerman, A. Salomaa, A. Sperduto, H. Enge, J. Ball, A. DiRienzo, S. Gazes, Yan Chen, J. D. Molitoris, and Mao Nai-feng, Phys. Rev. Lett. **45**, 1472 (1980).
[7]M. Beckerman, M. Salomaa, A. Sperduto, J. D. Molitoris, and A. DiRienzo, Phys. Rev. C **25**, 837 (1982).
[8]A. M. Stefanini, G. Fortuna, R. Pengo, W. Meczynski, G. Montagnoli, L. Corradi, A. Tivelli, S. Beghini, C. Signorini, S. Lunardi, M. Morando, and F. Soramel, Nucl. Phys. **A456**, 509 (1986).
[9]S. J. Skorka, A. M. Stefanini, G. Fortuna, R. Pengo, W. Meczynski, G. Montagnoli, A. Tivelli, S. Beghini, C. Signorini, and P. R. Pascholati, Z. Phys. A **328**, 355 (1987).
[10]S. Landowne, S. C. Pieper, and F. Videbaek, Phys. Rev. C **35**, 597 (1987).
[11]R. G. Stokstad, Y. Eisen, S. Kaplanis, D. Pelte, U. Smilanski, and I. Tserruya, Phys. Rev. Lett. **41**, 465 (1978).
[12]R. G. Stokstad, W. Reisdorf, K. D. Hildenbrand, J. V. Kratz, G. Wirth, R. Lucas, and J. Poitou, Z. Phys. A **295**, 269 (1980).
[13]R. G. Stokstad and E. E. Gross, Phys. Rev. C **23**, 281 (1981).
[14]W. Reisdorf, F. P. Hessberger, K. D. Hildebrand, S. Hofmann, G. Munzenberg, K. H. Schmidt, J. H. R. Schneider, W. F. W. Schneider, K. Summerer, G. Wirth, J. V. Kratz, and K. Schlitt, Phys. Rev. Lett. **49**, 1811 (1982).
[15]D. E. DiGregorio, J. O. Fernandez Niello, A. J. Pacheco, D. Abriola, S. Gil, A. O. Macciavelli, J. E. Testoni, P. R. Pascholati, V. R. Vanin, R. Liguori Neto, N. Carlin Filho, M. M. Coimbra, P. R. S. Gomes, and R. G. Stokstad, Phys. Lett. B **176**, 322 (1986).
[16]D. E. DiGregorio, M. diTada, D. Abriola, M. Elgue, A. Etchegoyen, M. C. Etchegoyen, J. O. Fernandez Niello, A. M. J. Ferrero, S. Gil, A. O. Macchiavelli, A. J. Pacheco, J. E. Testoni, P. R. Silveira Gomes, V. R. Vanin, R. Liguori Neto, E. Crema, and R. G. Stokstad, Phys. Rev. C **39**, 516 (1989).
[17]G. M. Berkowitz, P. Braun-Minzinger, J. S. Karp, R. H. Freifelder, T. R. Renner, and H. W. Wilschut, Phys. Rev. C **28**, 667 (1983).
[18]R. Butsch, J. Jänsch, D. Krämer, K.-H. Möbius, W. Ott, E. Steffens, G. Tungate, A. Weller, K. Becker, K. Blatt, H. C. Leucker, W. Luck, D. Fick, and P. Paul, Phys. Rev. C **36**, 1351 (1987).
[19]H. Esbensen, Nucl. Phys. **A352**, 147 (1981).
[20]C. H. Dasso, S. Landowne, and A. Winther, Nucl. Phys. **A405**, 381 (1983).
[21]M. J. Rhoades-Brown, P. Braum-Munzinger, M. Prakash, and S. Sen, in *Proceedings of the International Conference on Fusion Reactions Below the Coulomb Barrier, Massachusetts Institute of Technology, Cambridge, 1984,* Vol. 219 of *Lecture Notes in Physics* (Ref. 2), p. 162.
[22]R. A. Broglia, C. H. Dasso, and S. Landowne, Phys. Rev. C **32**, 1426 (1985).
[23]C. H. Dasso and S. Landowne, Phys. Lett. B **183**, 141 (1987).
[24]S. Landowne, S. C. Pieper, and F. Videbaek, Phys. Rev. C **35**, 597 (1987).
[25]O. Tanimura, Z. Phys. A **327**, 413 (1987).
[26]S. Landowne and J. R. Nix, Nucl. Phys. **A368**, 352 (1981).
[27]C. E. Aguiar, V. C. Barbosa, L. F. Canto, and R. Donangelo, Nucl. Phys. **A472**, 571 (1987).
[28]J. J. Vega, E. F. Aguilera, G. Murillo, J. J. Kolata, and A. Morsad (unpublished).
[29]C. Van Der Leun, D. M. Sheppard, and P. M. Endt, Nucl. Phys. **A100**, 316 (1967).
[30]D. Dehnhard, Phys. Lett. **38B**, 389 (1972).
[31]R. Weber, B. Jeckelmann, J. Kern, U. Kiebele, B. Aas, W. Beer, I. Beltrami, K. Bos, G. De Chambrier, P. F. A. Goudsmit, H. J. Leisi, W. Ruckstuhl, G. Strassner, and A. Vacchi, Nucl. Phys. **A377**, 361 (1982).
[32]D. Schwalm, E. K. Warburton, and J. W. Olness, Nucl. Phys. **A239**, 425 (1977).
[33]V. H. Thankappan, Phys. Rev. **141**, 957 (1966).
[34]D. Evers, J. Hertel, T. W. Retz-Schmidt, and S. J. Skorka, Nucl. Phys. **A91**, 472 (1967).
[35]D. Ardouin, R. Tamisier, M. Vergnes, G. Rotbard, J. Kalifa, G. Berrier, and B. Grammaticos, Phys. Rev. C **12**, 1745 (1975).
[36]D. Ardouin, B. Remaud, K. Kumar, F. Guilbault, P. Avignon, R. Seltz, M. Vergnas, and G. Rotbard, Phys. Rev. C **18**, 2739 (1978).
[37]R. Lecomte, M. Irshad, S. Landsberger, P. Paradis, and S. Monaro, Phys. Rev. C **22**, 1530 (1980).
[38]R. Lecomte, M. Irshad, S. Landsberger, G. Kajrys, P. Paradis, and S. Monaro, Phys. Rev. C **22**, 2420 (1980).
[39]R. Lecomte, G. Kajrys, S. Landsberger, P. Paradis, and S. Monaro, Phys. Rev. C **25**, 2812 (1982).
[40]M. Beckerman, M. K. Salomaa, J. Wiggins, and R. Rohe, Phys. Rev. C **28**, 1963 (1983).
[41]S. Sen, S. E. Darden, R. C. Luhn, N. O. Gaiser, G. Murillo, and J. Ramirez, Phys. Rev. C **31**, 787 (1985).
[42]F. Ballester, E. Casal, and J. B. A. England, Nucl. Phys. **A490**, 227 (1988).
[43]D. Goutte, *Proceedings of the International Conference on Nuclear Shapes, Crete, Greece,* 1987, edited by D. Garrett *et al.* (World Scientific, Singapore, 1988), p. 36.
[44]J. J. Vega, E. F. Aguilera, G. Murillo, and J. J. Kolata, Notas Fis. **10**, 335 (1987).
[45]E. F. Aguilera, J. J. Vega, E. Martinez, J. J. Kolata, and A. Morsad, Rev. Mex. Fis. **35**, 489 (1989).
[46]C. Y. Wong, Phys. Rev. Lett. **31**, 766 (1973).
[47]C. H. Dasso and S. Landowne, Phys. Lett. B **183**, 141 (1987).
[48]CCFUS code, modified by J. Fernandez Niello; S. Landowne (private communication).
[49]P. M. Endt, At. Data Nucl. Data Tables **23**, 3 (1979).
[50]P. M. Endt, At. Data Nucl. Data Tables **23**, 547 (1979).
[51]S. Raman, C. H. Malarkey, W. T. Milner, C. W. Nestor, Jr., and P. H. Stelson, At. Data Nucl. Data Tables **36**, 1 (1987).
[52]C. M. Perey, R. J. Silva, J. H. Dickens, and F. G. Perey, Phys. Rev. C **22**, 468 (1970).
[53]R. H. Spear, At. Data Nucl. Data Tables **42**, 55 (1989).
[54]M. M. King, Nucl. Data Sheets **51**, 161 (1987).
[55]B. Singh and D. A. Viggars, Nucl. Data Sheets **42**, 233 (1984).
[56]R. A. Broglia and F. Barraco, in *Proceedings of the International Conference on Fusion Reactions Below the Coulomb Barrier, Massachusetts Institute of Technology, Cambridge, 1984,* Vol. 219 of *Lecture Notes in Physics* (Ref. 2), p. 196.
[57]B. Singh and D. A. Viggars, Nucl. Data Sheets **51**, 225 (1987).
[58]P. Raghavan, At. Data Nucl. Data Tables **42**, 189 (1989).